

## MULTIPLE DOPPLER RADAR AND PROFILER ANALYSIS OF AN INTENSE WAKE LOW EVENT

Kevin R. Knupp and Timothy A. Coleman  
The University of Alabama, Huntsville, Alabama

### 1. INTRODUCTION

On 13 April 2009 an extensive and intense wake low event occurred over northeastern Mississippi, northern Alabama, and northern and central GA, at the trailing (western) edge of a mesoscale convective system (MCS). This was a significant weather event, as many trees were toppled over this large region, some onto homes and vehicles. Approximately 150,000 Alabama Power customers lost power and power outages of a similar magnitude also occurred in Georgia. Structural damage occurred, and one fatality was reported.

A wind gust of  $26 \text{ m s}^{-1}$  was recorded in downtown Birmingham, AL, with gusts  $> 20 \text{ m s}^{-1}$  common over the entire region mentioned above. Winds in excess of  $15 \text{ m s}^{-1}$  persisted at many locations for one hour or more. Pressure falls of 8-10 hPa were common, and multiple high amplitude pressure oscillations were measured by surface stations. Even though the main wake low was propagating toward the southeast, additional gravity waves appeared to be propagating toward the NE in the wake low region, causing superposed pressure, wind, and moisture oscillations.

This paper will focus on the kinematic structure of the stratiform region where the strong winds were generated. This will be accomplished using data from multiple WSR-88D radars, dual Doppler radar analyses using the KHTX WSR-88D and ARMOR radars (70 km baseline), vertical profile data from the MIPS (wind profiles from a 915 MHz wind profiler; and temperature and humidity profiles from a microwave profiling radiometer), and surface and sounding data. The pressure oscillations were accompanied by waves analyzed in time-height sections of vertical motion, potential temperature, and mixing ratio calculated from MIPS measurements. These data will be used to address the theory of wake lows and to attempt to determine their similarity to gravity waves. Additional wave features, possibly ducted

gravity waves, were superposed over the wake low, and these will also be examined.

### 2. REVIEW OF WAKE LOWS

There have been numerous cases discussed in the literature of wake lows causing high winds and sometimes wind damage (e.g., Bosart and Seimon 1988; Koch and O'Handley 1997; Bradshaw et al. 1999; Koch and Saleeby 2001). The surface winds in wake lows and gravity waves are primarily caused by transient mesoscale pressure gradients, producing highly ageostrophic winds. A recent paper by Coleman and Knupp (2009) discusses the conditions governing the damaging wind potential in a particular wake low, including intrinsic propagation speed, background wind, and amplitude.

Wake lows were first examined in multiple works by Fujita (1955, 1959, 1963), and others (e.g., Brunk 1953; Williams 1953). They are typically located at or near the back edge of the

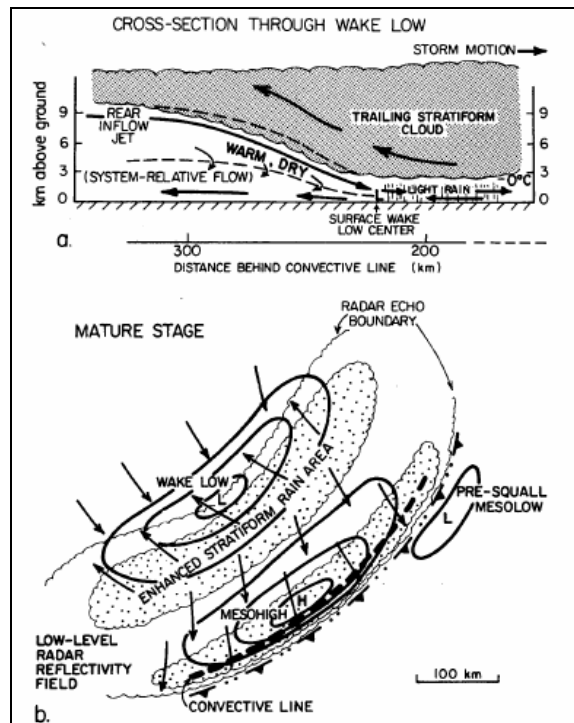


**Figure 1.** a) Cross section through a wake low; b) plan view of MCS with wake low (from Johnson and Hamilton 1988)

\*Corresponding Author Address: Kevin Knupp, Atmospheric Science Department, The University of Alabama in Huntsville, 320 Sparkman Drive, Huntsville, AL 35805; Email: kevin@sstc.uah.edu.

trailing stratiform precipitation region of an MCS (e.g., Johnson and Hamilton 1988), and are often associated with a sharp gradient in radar reflectivity factor due to subsidence (e.g., Stumpf et al. 1991; Johnson et al. 1989).

Figure 1 (from Johnson and Hamilton 1988) has become a commonly shown schematic of a wake low. The mesoscale low pressure area behind the MCS is associated with subsidence-induced warming and reduced hydrostatic pressure, and the subsidence may be associated with a descending rear-inflow jet (e.g., Johnson and Hamilton 1988; Stumpf et al. 1991). Stumpf et al. (1991) proposed that dry air in a rear-inflow jet (RIJ) may cool rapidly once it encounters the stratiform precipitation region, through evaporation. This cool air would then descend rapidly due to negative buoyancy, eventually overshooting at low-levels, or becoming positively buoyant while still descending. It should be noted that vertical motion in statically stable air causes larger pressure perturbations at the surface when the motion is at low levels, where the density is highest (Coleman 2008; Trexler and Koch 2000). Therefore, a mesoscale area of positively buoyant air would produce a local but potentially high amplitude pressure minimum at the surface.

A connection between gravity waves and the subsidence in wake lows was proposed by Schmidt and Cotton (1990). Others (e.g., Haertel and Johnson 2000; Pandya and Durran 1996) also discuss the possible similarities between wake lows, and their parent MCS, with gravity waves. Therefore, it is possible that wake lows are indeed similar to gravity waves.

### 3. DATA

We utilize data from two WSR-88D radars, KBMX and KHTX (two others, KGWX and KFCC will be included in the future), the ARMOR radar, the Mobile Integrated Profiling System (MIPS), and surface data (ASOS and other). Relative locations of these instruments are shown in Fig. 2. The KHTX/ARMOR combination provides a dual Doppler capability (over a 70 km baseline) for retrieval of boundary layer flows in this case since the ARMOR conducted VAD scans at only three elevations, 0.7, 1.3 and 2.0 deg during the event, while the KHTX radar performed VCP-11 scans.

### 4. SYNOPTIC AND MESOSCALE ENVIRONMENT

The MCS of interest here formed in advance of a closed 500 mb trough centered over eastern Kansas on 13 April. The surface analysis (Fig. 3)

shows a surface cyclone located over Arkansas, with a relatively tight pressure gradient towards the east and northeast, including the area affected by the wake low.

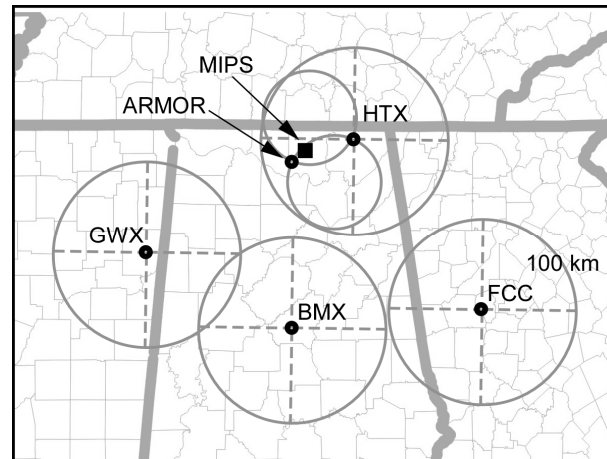


**Figure 2.** Locations of WSR-88D radars (HTX, GWX, BMX and FCC), the Advanced Radar for Operational and Meteorological Research (ARMOR), and the MIPS. Range rings of 100 km are drawn for the WSR-88D radars, and the dual Doppler lobes for ARMOR and HTX are also drawn as smaller circles.

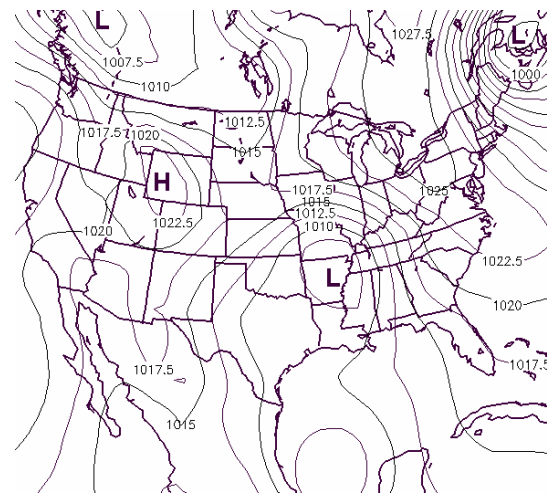


**Figure 3.** Analysis of sea level pressure at 0600 UTC 13 April 2009, derived from the NCEP/NCAR reanalysis.

### 5. THE WAKE LOW

Between 0200 and 1500 UTC, an intense wake low propagated from NE Mississippi, across northern and central Alabama, and into northern Georgia. The wake low was at the rear (western) edge of the stratiform precipitation associated with an MCS (Fig. 4). Interestingly, the MCS was preceded by a significant bore, as evidenced by the 3 hPa pressure rise at 2300 UTC, 12 April

(Fig. 5). Processes associated with the wake low produced a fairly sharp gradient in reflectivity at the back edge of the MCS precipitation region (see Figure 3). According to Coleman and Knupp (2009), the event had all the characteristics of a high-wind producing low pressure disturbance: (i) very pressure large amplitude, (ii) slow intrinsic propagation speed, and (iii) a background headwind. Damage reports were widespread (see Figure 6).

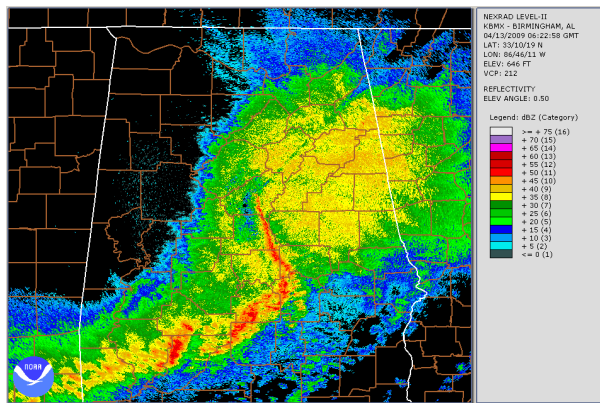


**Figure 4.** Radar reflectivity at 0622 UTC from the WSR-88D at Birmingham, Alabama (BMX).

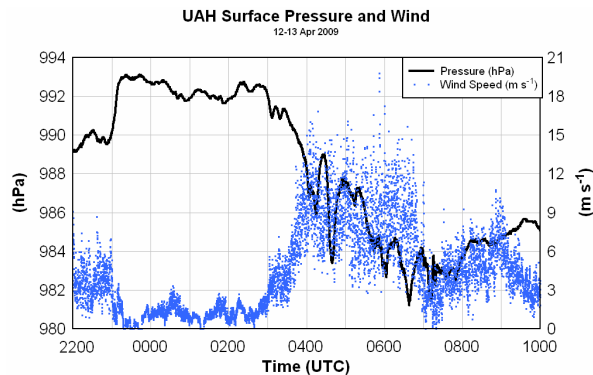


**Figure 5.** Time series of sea-level pressure (hPa, solid curve) and maximum wind gust ( $\text{m s}^{-1}$ , blue dots) at 1-minute resolution.

The pressure drops at the surface were large and rapid. In Figure 5, a time series of mean sea level pressure and wind gusts at the MIPS site on the UAH campus, one can see the large, overall pressure drop associated with the wake low. It began with a rapid 5 hPa pressure drop from 991 to 986 hPa in only 45 minutes between 0330 and 0415 UTC. The overall pressure drop continued until after 0630 UTC, when the pressure reached its minimum of 981 hPa. The additional, fairly large amplitude (up to 5 hPa) and short period (30-45 minutes) rises and falls in pressure that are superposed over the wake low are also apparent,

the most vigorous occurring around 0430 UTC, with others occurring around 0515, 0600, and 0634 UTC. Strong winds also lasted for a long period of time. Even at UAH, where winds were not as strong as they were at locations farther south, winds gusting above  $10 \text{ m s}^{-1}$  lasted for 3 hours, from 0345 through 0645 UTC, and a peak wind of  $20 \text{ m s}^{-1}$  occurred around 0555 UTC. About 100 km south of UAH, in Clay, AL, one-minute pressure observations shown in Fig. 7 indicate less superposed wave activity during the wake low, with a fairly uniform, large pressure drop of 8 hPa occurring between 0645 and 0800 UTC. One pressure rise/fall couplet was noted between 0800 and 0900 UTC.

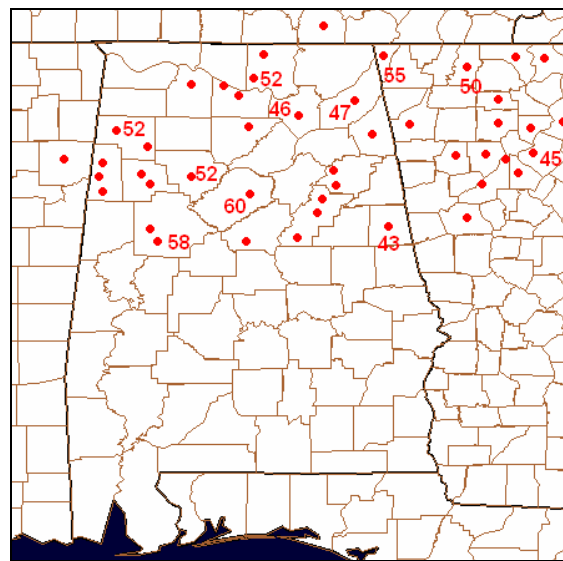


**Figure 6.** Locations of wind damage (red dots) and measured wind speeds (mph) on 13 Apr 2009

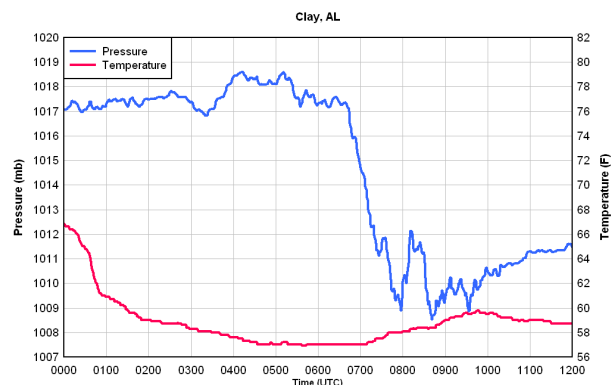


**Figure 7.** Surface pressure (hPa) and temperature (F) at Clay, AL, just NE of Birmingham.

A PPI Doppler velocity image from the BMX radar, along with cross sections of reflectivity and velocity (Figures 8-10), illustrate several flow

features. The fairly uniform, linear increase in outbound velocity (into the wake low) is noted in Fig. 8. Figure 9 shows the large reflectivity anvil above 4 km AGL behind the stratiform region. It extends at least 150 km behind the back edge of the rain at the surface. There is a large horizontal gradient in reflectivity between 30 km and 50 km away from the radar, consistent with subsidence and drying.

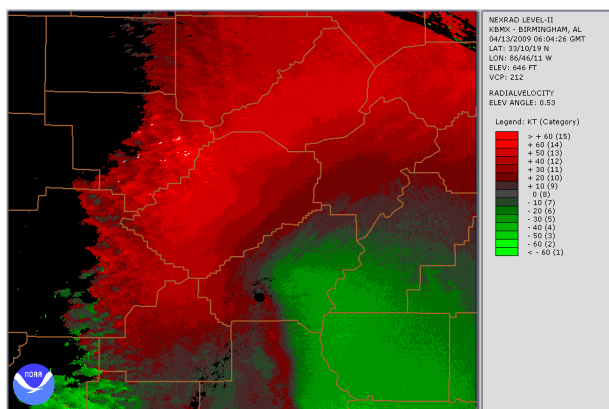


**Figure 8.** PPI scan at 0.5 degrees of Doppler velocity (kt) from the BMX WSR-88D radar at 0604 UTC.

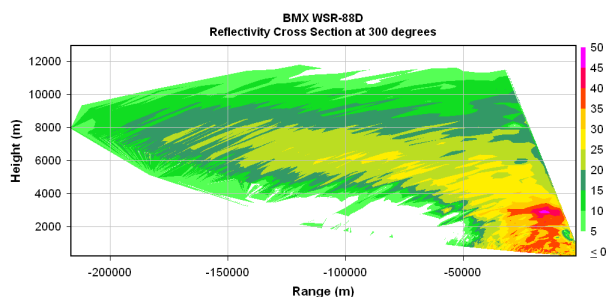


**Figure 9.** Cross-section along 300 degrees azimuth of reflectivity from BMX at 0604 UTC.

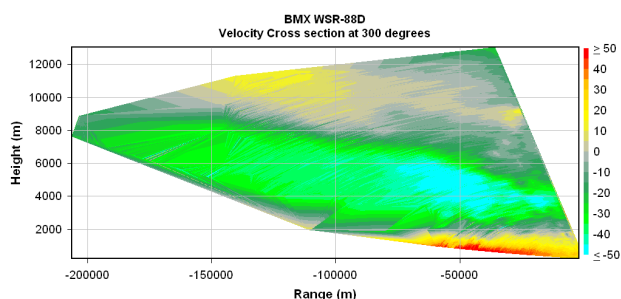


**Figure 10.** Cross-section along 300 degrees azimuth of velocity from BMX at 0604 UTC.

The velocity cross section in Fig. 10 shows a fairly intense rear inflow jet (RIJ) in and underneath the precipitation anvil aloft. The strongest part of the RIJ, with winds greater than

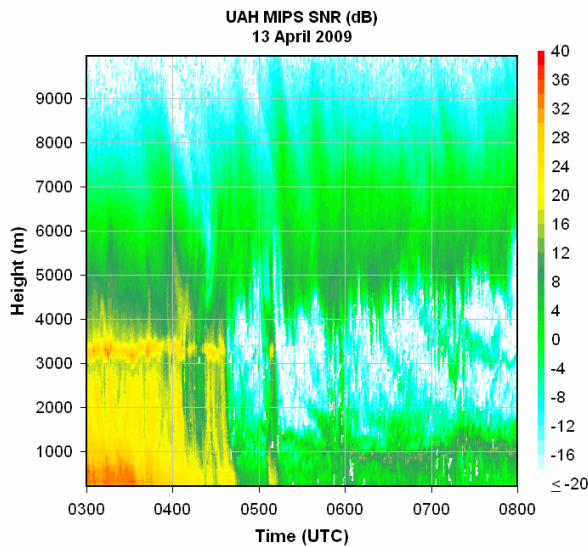
50 kt ( $25 \text{ m s}^{-1}$ ), descends from near 6 km AGL at 75 km range, to 4 km AGL at 40 km range. The RIJ then decreases somewhat in intensity inside 40 km range, indicating large horizontal convergence near 4 km AGL. The continuity equation requires vertical divergence here, so downward motion should be occurring below 4 km AGL. The strong outbound low-level winds are also shown in Figure 10, with a shallow (less than 1 km vertically) area of 40 kt or greater winds having large horizontal extent (about 50 km). The low-level winds peak very near the area of maximum convergence aloft. This would be consistent with subsidence warming and a surface pressure minimum below the convergence area. As shown by Coleman and Knupp (2009), the strongest winds for a propagating pressure disturbance occur at the location of the maximum magnitude of pressure perturbation, consistent with the impedance relation.

The RIJ location and weakening near the back edge of the precipitation area also indicates that evaporation of precipitation aloft may be producing cooling. This cooling aloft could also cause subsidence due to temporary negative buoyancy. However, once the air reaches the surface, it becomes positively buoyant and “overshoots” its equilibrium level, similar to a heat burst. This event did not, however, exhibit a heat burst signature, as surface temperatures remained near  $15\text{-}16^\circ\text{C}$  (Fig. 7).

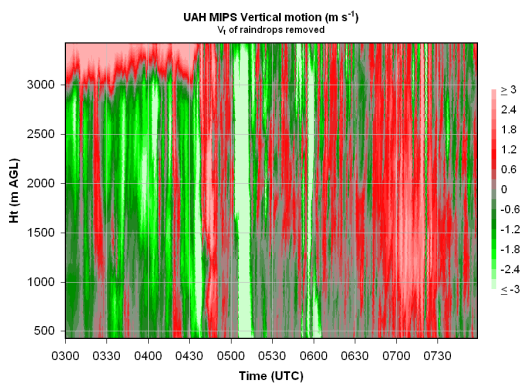
The MIPS 915 MHz profiler provides a better view of the wake low at lower levels, and also provides direct measurements of vertical motion (terminal fall speeds of raindrops were removed below 3400 m AGL, resulting in some errors). Figure 11, a time-height section of profiler signal-to-noise ratio (SNR) indicates a melting level near 3200 m AGL, and precipitation decreasing in intensity between 0300 and 0400 UTC. The decrease is occurring in a sloping pattern, with the precipitation seeming to end slightly aloft before it ends at lower levels. This may indicate that some of the precipitation is being evaporated by dry, warm air descending below the RIJ. The raindrops that reach the surface below the dry air must have had larger terminal fall speeds than the vertical motion of the air, not allowing the dry air to reach them before they reached the ground.

Figure 12 indicates downward vertical motion of  $1$  to  $3 \text{ m s}^{-1}$  over an increasingly deep layer between 0330 and 0430 UTC, corresponding to the time of the largest pressure drop at UAH (see Figure 4). The more intense upward and downward velocity perturbations associated with passing ducted gravity waves superposed on the

wake low also appear. The first significant perturbation occurs at 0415 UTC, as upward motion up to  $1 \text{ m s}^{-1}$  is associated with a rapid 3 hPa pressure rise. This upward motion is followed by downward motion greater than  $3 \text{ m s}^{-1}$ , and a sudden decrease in surface pressure of 5 hPa in only 15 minutes. This indicates a process in addition to the wake low. However, the average vertical motion in the lowest 3 km of the atmosphere between 0300 and 0600 UTC is downward, and this is consistent with the overall 9 hPa pressure drop shown in Figs. 5 and 7 around this time.



**Figure 11.** Time-height section of MIPS 915 MHz profiler signal-to-noise ratio (dB).



**Figure 12.** Time-height section of MIPS 915 MHz profiler vertical motion ( $\text{m s}^{-1}$ ), with the terminal fall speed of raindrops removed.

## 5. ADDITIONAL DETAILS ON FLOW AND WAVE FEATURES

The high frequency pressure fluctuations, indicated between 0400 and 0700 UTC at the MIPS site (Fig. 5), were associated with distinct features (some linear) in reflectivity factor observed by the KHTX and ARMOR radars along the northern periphery of the stratiform precipitation. Figures 13 and 14 present  $Z$  and  $V_r$  images from KHTX around the times of the significant short-period pressure variations at 0419 and 0528 UTC. At 0419 UTC both linear and curvilinear structures are indicated in the  $Z$  patterns at 0.5 deg around the MIPS. These are associated with appreciable variations in  $V_r$  along the HTX radial passing over the MIPS site. At this time, the ARMOR  $V_r$  measurements (not shown) indicated strong ( $25 \text{ m s}^{-1}$ ) flow just above the surface. Figure 14 shows the KHTX patterns at 0529 UTC. By this time, a pair of linear features were located northwest of KHTX, detached from the main body of stratiform precipitation and moving towards the NE. The low-level flow is highly sheared, as low level winds at the ARMOR exceed  $25 \text{ m s}^{-1}$  from the southeast (also at KHTX). This strong SE flow is capped by winds up to  $40 \text{ m s}^{-1}$  within the 3-4 km layer as shown in Fig. 14b. Based on this, we hypothesize that the prominence of gravity waves is related to initiation via a Kelvin-Helmholtz shearing instability. Subsequent dual Doppler analysis of the boundary layer flow, along with VAD and more detailed single Doppler analyses, will yield additional insights on the characteristics of the highly variable flow within what is generally considered to be a stratiform region with smoothly-varying quasi-laminar flows. In this case the flow is quite variable and apparently filled with waves and turbulence.

## 6. SUMMARY AND CONCLUSIONS

This paper has presented a preliminary study of an intense wake low event associated with the trailing region of a mesoscale convective system. This wake low generated strong surface winds over a large geographical region, producing widespread power outages over between northern Mississippi and central Georgia.

The MCS did not exhibit a leading line of deep convection throughout its entire N-S extent. The wake low was most intense on the northern periphery of the MCS where stratiform precipitation was prevalent. In contrast, the most intense deep convection was located over the

southern half of the MCS from central to southern Alabama. An intense mid-level westerly inflow jet exceeding  $40 \text{ m s}^{-1}$  (ground relative) formed within the 3-4 km AGL layer, and its descent appeared to generate the low surface pressure with perturbation values up to 8-10 mb over a horizontal extent of 100-200 km. The induced pressure gradient produced widespread southeasterly surface winds with gusts of  $25\text{-}30 \text{ m s}^{-1}$ . Along the northern to western periphery of the MCS, a large shear zone between the midlevel inflow jet ( $40 \text{ m s}^{-1}$ ) and low level southeasterly flow ( $25\text{-}30 \text{ m s}^{-1}$ ) apparently generated high values of vertical shear, and hence gravity waves that were superimposed on the longer period wake low. The new finding in this case is the presence of high amplitude, short period gravity waves superimposed on a larger scale wake low.

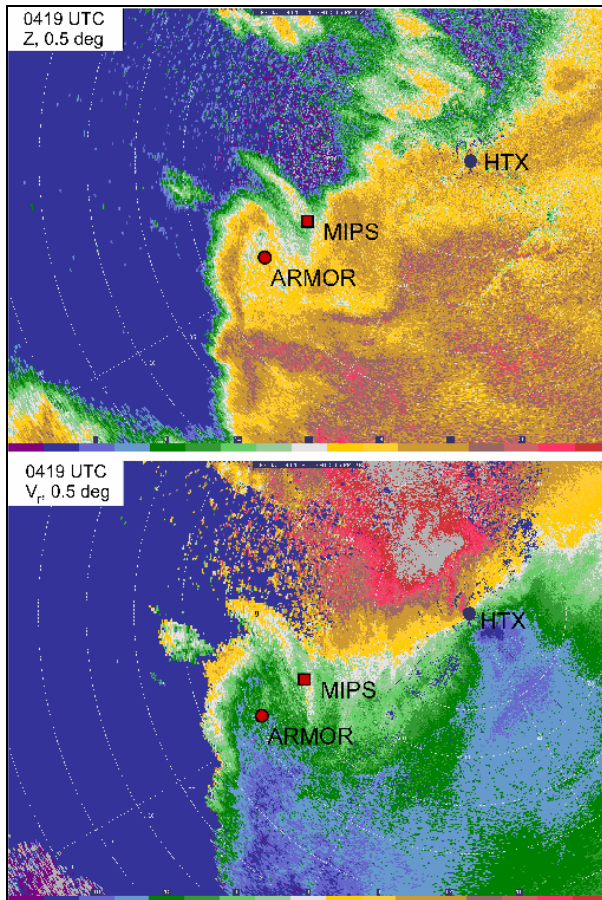


**Figure 13.** PPI of reflectivity factor (top) and radial velocity (bottom) at 0.5 deg elevation angle from KHTX at 0419 UTC. Locations of the MIPS and MAX relative to the KHTX radar are shown. Range rings are drawn every 15 km, starting at 30 km. Both Z and  $V_r$  exhibit considerable horizontal variability, even though this region is technically a stratiform region of the MCS.

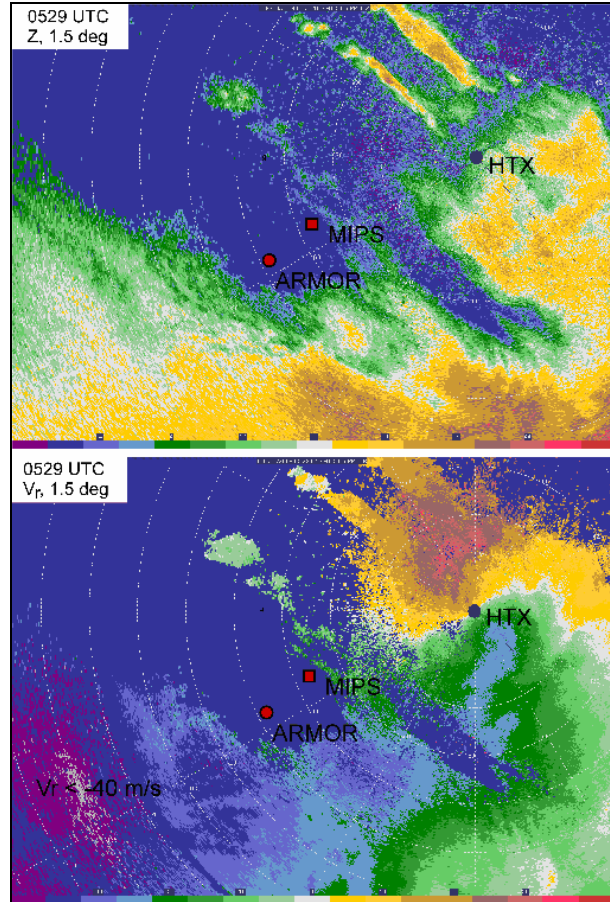


**Figure 14.** Same as Fig. 14, except for 1.5 deg elevation at 0529 UTC. In this case, the shear between inflow greater than  $40 \text{ m s}^{-1}$  in the bottom level (3-4 km AGL), and the  $30 \text{ m s}^{-1}$  SE flow near the surface (close to the HTX radar) is apparent.

Future work will include a more detailed single Doppler analysis of radar data from the WSR-88D radars, a dual Doppler analysis of boundary layer airflow over a 100 domain of northern Alabama. This analysis will examine in more detail the structure of the both the wake low and embedded gravity waves in order to better understand their forcing and dynamics.

#### **Acknowledgements**

*This research was supported by NOAA under grant NA08OAR4600896.*

## References

- Bosart, L.F., and A. Seimon, 1988: A case study of an unusually intense atmospheric gravity wave. *Mon. Wea. Rev.*, **116**, 1857–1886.
- Bradshaw, J. T., R. A. Murphy, and K. J. Pence, 1999: The Alabama gravity wave event of February 22, 1998: A classic mesoscale forecasting challenge. *8th Conf. on Mesoscale Proc.*, American Meteorological Society.
- Brunk, I. W., 1953: Squall lines. *Bull. Amer. Meteor. Soc.*, **34**, 1-9.
- Coleman, T.A., and K. R. Knupp, 2009: Factors Affecting Surface Wind Speeds in Gravity Waves and Wake Lows. *Weather and Forecasting*: In Press.
- Coleman, T. A., 2008: The interactions of gravity waves with mesocyclones and tornadoes. Ph. D. dissertation, The University of Alabama in Huntsville, 220 pp.
- Fujita, T. T., 1955: Results of detailed synoptic studies of squall lines. *Tellus*, **7**, 405-436.
- Fujita, T. T., 1959: Precipitation and cold air production in mesoscale thunderstorm systems. *J. Meteor.*, **16**, 454-466.
- Fujita, T. T., 1963: Analytical mesometeorology. A review. *Meteor. Monogr.*, **5**, 77-125.
- Haertel, P. T., and R. H. Johnson, 2000: The linear dynamics of squall line mesohighs and wake lows. *J. Atmos. Sci.*, **57**, 93-107.
- Johnson, R.H., and P.J. Hamilton, 1988: The relationship of surface pressure features to the precipitation and airflow structure of an intense midlatitude squall line. *Mon. Wea. Rev.*, **116**, 1444–1473.
- Johnson, R. H., S. Chen, and J. J. Toth, 1989: Circulations associated with a mature-to-decaying midlatitude mesoscale convective system. Part I: Surface features – Heat bursts and mesolow development. *Mon. Wea. Rev.*, **117**, 942-959.
- Koch, S. E., and C. O'Handley, 1997: Operational forecasting and detection of mesoscale gravity waves. *Wea. Forecasting*, **12**, 253-281.
- Pandya, R.E., and D.R. Durran, 1996: The influence of convectively generated thermal forcing on the mesoscale circulation around squall lines. *J. Atmos. Sci.*, **53**, 2924–2951.
- Schmidt, J.M., and W.R. Cotton, 1990: Interactions between upper and lower tropospheric gravity waves on squall line structure and maintenance. *J. Atmos. Sci.*, **47**, 1205–1222.
- Stumpf, G. J., R. H. Johnson, and B. F. Smull, 1991: The wake low in a midlatitude mesoscale convective system having complex convective organization. *Mon. Wea. Rev.*, **119**, 134–158.
- Trexler, C.M., and S.E. Koch, 2000: The Life Cycle of a Mesoscale Gravity Wave as Observed by a Network of Doppler Wind Profilers. *Mon. Wea. Rev.*, **128**, 2423–2446.
- Williams, D.T., 1953: Pressure wave observations in the central Midwest, 1952. *Mon. Wea. Rev.*, **81**, 278–289.